Unified Modelling of Wave-Propelled USVs Using Closed-Form Expressions

Andreas Gudahl Tufte [*,1] **Tor Arne Johansen** [*]
Morten Breivik [*] **Andrew Ross** [**]

[*] *Department of Engineering Cybernetics, Norwegian University of Science and Technology (NTNU), NO-7491, Trondheim, Norway.*
[**] *SINTEF Ocean, NO-7465, Trondheim, Norway.*

Abstract: This paper presents a physics-based unified modelling framework for wave-propelled uncrewed surface vehicles (USVs), combining manoeuvring, seakeeping, and wave-propulsion models into a cohesive architecture. The model is intended for a range of wave-propelled USVs, and is provided with closed-form expressions. A case study on a 5-meter AutoNaut vehicle demonstrates the model's ability to reproduce realistic propulsion behaviour, and supports design of guidance and decision support systems for long-endurance ocean navigation.

Keywords: Autonomous surface vehicles, Wave propulsion, Unified model architecture

1. INTRODUCTION

Wave energy offers an advantage over traditional sails for green propulsion due to its typically lower variability, as waves propagate more uniformly across oceans from distant sources. There are new and exciting applications, e.g., for long-endurance remote oceanographic monitoring without human intervention, see, e.g., (Bøckmann, 2015).

The primary method employed in wave-propelled vehicles involves the use of lift-generating foils. The foils are typically mounted on struts attached to the hull, and the relative motion between the foil and the water is transferred into propulsive thrust. This will in principle allow the vehicle to operate with an unrestricted endurance, if not for factors such as maintenance, strong ocean currents and limited energy storage/harvesting for electric systems.

A challenge for autonomous operations using wave propulsion, e.g. on uncrewed surface vehicles (USVs), is that the forward speed relies on the environmental sea state and is not actively controlled. The controller running on the vehicle needs to perform well in various environmental conditions. Often, such path-controllers are based on a 3-degree-of-freedom (DOF) manoeuvring model which is unsuited as a stand-alone model to include predictions for the propelled thrust. In (Dallolio et al., 2022b) a course controller was designed and tested for the AutoNaut vehicle and they concluded that "*a speed model is key and would provide useful knowledge used for mission planning and course control*". As shown in (Dallolio et al., 2022a), such speed models can be effectively used to improve control performance through gain scheduling.

Accurate hydrodynamic models for such vehicles are hard to derive analytically due to the coupled viscous interaction of the foils and the hull. Øveraas et al. (2022) utilized data-driven methods for predicting the speed using metocean forecasting, but one is left reliant on forecasting to predict the motion. Recent development by Mounet et al. (2024) provided a novel method for estimation of the seakeeping motion of USVs based on explicit closed-form expressions with experimental validation.

[1] Corresponding author: andreas.tufte@ntnu.no

Unlike data-driven methods and motivated by literature, (1) we generalize a physics-based speed model for wave-propelled USVs with real-time applicability by extending the unified time-domain model given by Fossen (2005), (2) presents new contributions for modelling forces on the foils in previously non-modelled operating conditions, and (3) demonstrate usability in a case-study with previously studied manoeuvring models, recent seakeeping models and the refinements in foil modelling from this paper.

2. UNIFIED MODEL STRUCTURE

We propose a model for wave-propelled USVs by the superposition and interaction of three subsystems given in Fig. 1. The 6-DOF rigid body motion of the USV, which also needs to incorporate the presence of the foils, can be decomposed into a manoeuvring model Σ_1 depending on a parameter vector $\boldsymbol{\alpha}_1$ for *surge*, *sway* and *yaw* and a seakeeping model Σ_2 depending on $\boldsymbol{\alpha}_2$ for *heave*, *roll* and *pitch*. This is the classical unified model as described by Fossen (2005). The architecture is supplemented by a cohesive propulsion subsystem Σ_3 (with $\boldsymbol{\alpha}_3$) to include the additional DOFs for modelling propulsive forces and *foils*.

3. MANOEUVRING MODEL

The 3-DOF dynamical model for the horizontal-plane motion is well-known and a complete derivation is found in (Fossen, 2021). The position (x^n, y^n) and cardinal heading ψ of the USV in North-East-Down (NED) reference frame is denoted by $\boldsymbol{\eta} = [x^n, y^n, \psi]^\top$. The subsystem Σ_1 is

$$\dot{\boldsymbol{\eta}} = \mathbf{R}(\psi)\boldsymbol{\nu}, \tag{1a}$$

$$\mathbf{M}\dot{\boldsymbol{\nu}}_\mathrm{r} + \mathbf{C}(\boldsymbol{\nu}_\mathrm{r})\boldsymbol{\nu}_\mathrm{r} + \mathbf{B}(\boldsymbol{\nu}_\mathrm{r})\boldsymbol{\nu}_\mathrm{r} = \boldsymbol{\tau}_\mathrm{env} + \boldsymbol{\tau}_\mathrm{RB}. \tag{1b}$$

Here, the velocity vector $\boldsymbol{\nu} = \boldsymbol{\nu}_\mathrm{r} + \boldsymbol{\nu}_\mathrm{c} = [u, v, r]^\top$ is the body frame velocity in *surge*, *sway* and *yaw*, where $\boldsymbol{\nu}_\mathrm{c} = [u_c, v_c, 0]^\top$ is the sea current velocity assumed to be irrotational and slowly varying, and $\boldsymbol{\nu}_\mathrm{r} = [u_r, v_r, r]^\top$ is the relative velocity through the water. The matrices are the mass matrix $\mathbf{M} = \mathbf{M}_\mathrm{RB} + \mathbf{M}_\mathrm{A} \succ \mathbf{0}$, which includes inertia of the rigid body (assumed constant) and added mass, the Coriolis and centripetal matrix $\mathbf{C} = \mathbf{C}_\mathrm{RB} + \mathbf{C}_\mathrm{A} = -\mathbf{C}^\top$, which includes rigid body and hydrodynamic components, and the damping matrix $\mathbf{B}$ ensures dissipative motion

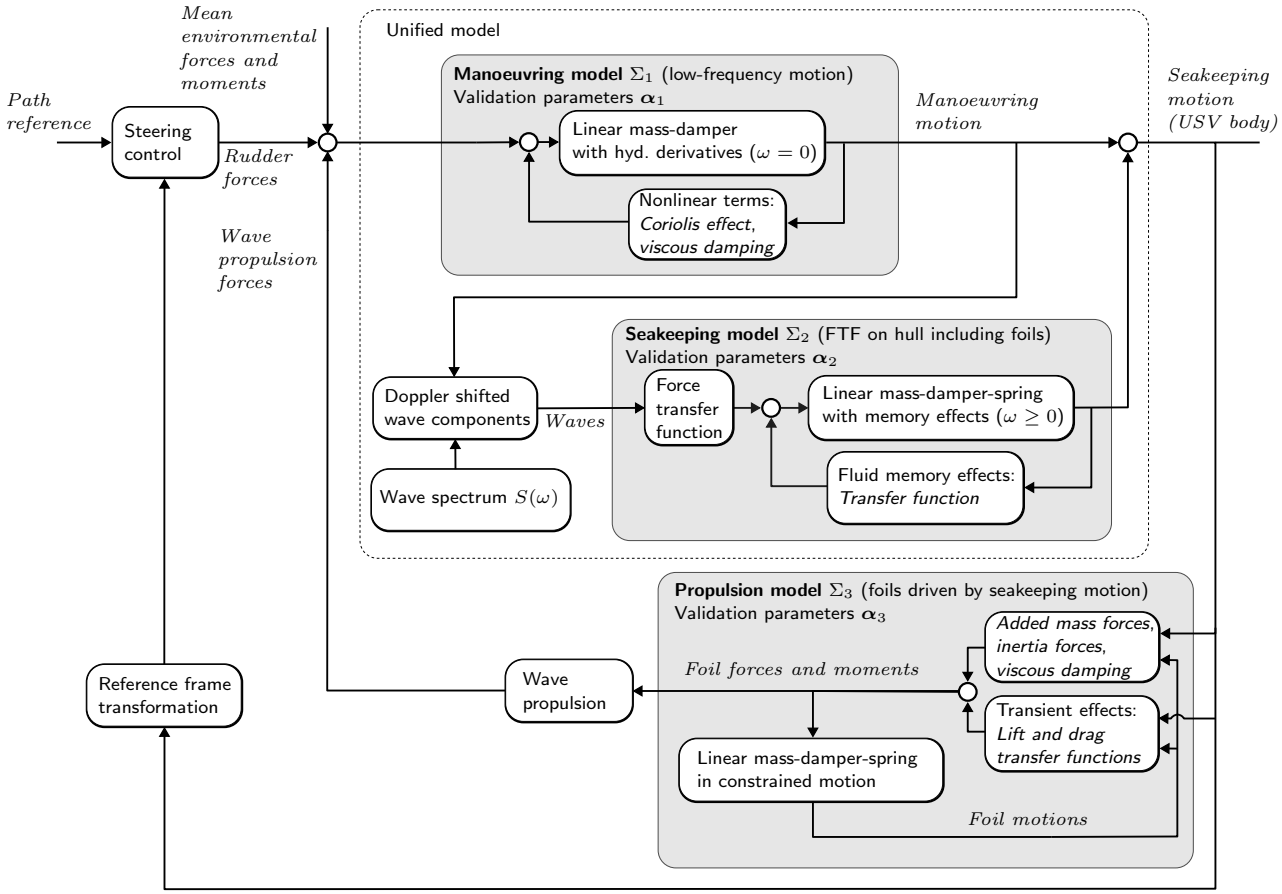

Fig. 1. Time-domain model architecture with superposition of a manoeuvring model Σ_1, seakeeping model Σ_2 and the extended propulsion model Σ_3 of the foils driven by the relative motion of the USV and water. Wave propulsion forces are fed back to the manoeuvring model. Architecture inspired by Fossen (2005).

through the water. Wind and mean second-order wave forces are included in the generalized environmental forces, $\boldsymbol{\tau}_{\text{env}} = \boldsymbol{\tau}_{\text{wind}} + \boldsymbol{\tau}_{\text{wave2}}$. Lastly, the rigid body forces $\boldsymbol{\tau}_{\text{RB}}$ comprises the steering and propulsion forces from rudder, $\boldsymbol{\tau}_{\text{rudd}}$, which is actively controlled, an optional propeller for safety interventions (not included in the analysis), and the wave-propulsion forces by the foils $\boldsymbol{\tau}_{\text{foil}}$. The rotation matrix $\mathbf{R}(\psi)$ rotates coordinates from the NED frame to the manoeuvring frame for Σ_1 in which velocities are given.

3.1 Parameters in the manoeuvring model

The matrices in the manoeuvring model depend on the specific USV, which e.g., can be modelled as a 3-DOF surge-decoupled representation, see (Fossen, 2021). The following parameters may describe subsystem Σ_1:

$$\boldsymbol{\alpha}_1 = \big(m, J_z, x_g, \text{parameters in manoeuvring matrices, etc.}\big)$$

Here, m is the vehicle mass, J_z is the moment of inertia in yaw and x_g is the longitudinal position of centre of gravity.

The parameters in $\boldsymbol{\alpha}_1$–$\boldsymbol{\alpha}_3$ for subsystems Σ_1–Σ_3 should be adjusted according to the accuracy of model, and validation of these parameters is outside the scope of the paper.

- *Wind*: For rapid estimation of wind forces, see e.g., (Brix, 1993). Low-order models has been given by Fossen (2021).
- *Rudder*: For rudder forces, see e.g., Kijima et al. (1990).

4. SEAKEEPING MODEL

We use the method inspired by Jensen et al. (2004) and Mounet et al. (2024) in order to predict motion in *heave*, *roll* and *pitch* for wave-propelled vehicles. The model uses semi-empirical force transfer functions (FTFs) derived from a monohull geometry by length $\tilde{L}$, breadth $\tilde{B}$ and draft $\tilde{T}$, see Fig. 2b. It is expected that these dimensions are equal or greater than the vehicle's actual ones to incorporate added viscous damping from the foils. Note that the seakeeping motion is found by the combination of motion output of Σ_1 and Σ_2 (by extending to full state vectors with zeros for non-modeled states). We model the wave-induced motions Σ_2 (with abuse of notation) by

$$\mathbf{M}_{\text{rao}}(\omega)\ddot{\boldsymbol{\xi}} + \mathbf{B}_{\text{rao}}(\omega)\dot{\boldsymbol{\xi}} + \mathbf{C}_{\text{rao}}\boldsymbol{\xi} = \boldsymbol{\tau}_{\text{wave1}}. \tag{2}$$

Here, the *heave*, *roll* and *pitch* is $\boldsymbol{\xi} = [z^n, \phi, \theta]^\top$, the wave frequency ω, and the motion is driven by the first-order wave forces $\boldsymbol{\tau}_{\text{wave1}}$, defined by forcing functions later. We need to introduce the approximate state-space version of Eq. (2) suitable for numerical implementation (based on the time-domain representation; see Ogilvie (1964))

$$\mathbf{M}_{\text{rao}}(\infty)\ddot{\boldsymbol{\xi}} + \mathbf{B}_{\text{rao}}(\infty)\dot{\boldsymbol{\xi}} + \boldsymbol{\mu}_{\text{r}} + \mathbf{C}_{\text{rao}}\boldsymbol{\xi} = \boldsymbol{\tau}_{\text{wave1}}, \tag{3a}$$

$$\dot{\mathbf{x}}_{\text{r}} = \mathbf{A}_{\text{r}}\mathbf{x}_{\text{r}} + \mathbf{B}_{\text{r}}\dot{\boldsymbol{\xi}}, \tag{3b}$$

$$\boldsymbol{\mu}_{\text{r}} = \mathbf{C}_{\text{r}}\mathbf{x}_{\text{r}}, \tag{3c}$$

where the fluid memory effects is given by the vector $\boldsymbol{\mu}_{\text{r}}$ driven by the velocity $\dot{\boldsymbol{\xi}}$, see Kristiansen and Egeland (2003). A strength in the analysis is that we show that the inertia matrix $\mathbf{M}_{\text{rao}}$, damping matrix $\mathbf{B}_{\text{rao}}$ and restoring matrix $\mathbf{C}_{\text{rao}}$ can be modelled as diagonal matrices.

For a range of wave-propelled USVs, the roll motion may be neglected such that only the pitch and heave motion is the main driver of the wave-propulsion system Σ_2. When a

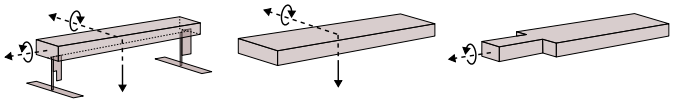

(a) Actual geometry (b) Heave and pitch (c) Roll model

Fig. 2. Simplified monohull geometries for modelling wave-induced motions in subsystem Σ_2.

5-DOF seakeeping motion is used to model wave-propelled USVs, the parameter for subsystem Σ_2 reduces to only

$$\boldsymbol{\alpha}_2 = \left(\tilde{L}, \tilde{B}, \tilde{T}\right).$$

4.1 Wave encounter frequency

We denote the wave encounter angle $\beta = \beta_k - \psi$ for waves propagating in cardinal direction β_k such that 0° corresponds to following waves, 90° to beam waves and 180° to head waves, see Fig. 3. The encounter frequency ω_e differs from the intrinsic wave frequency ω due to the vehicle's speed and heading, and is the proper frequency used in the FTF in Eq. (2) and the following subsections.

From the manoeuvring speed $U = \sqrt{u^2 + v^2}$ and the deep water dispersion relation, $\omega^2 = gk$, k being the wave number and g the gravitational constant, the Doppler shifted encounter frequency is (where $\eta := \omega_e/\omega$)

$$\omega_e = \left|\omega - (\omega^2/g)U\cos(\beta)\right| = \eta\,\omega. \tag{4}$$

4.2 Pitch and heave motion

The closed-form expressions for the longitudinal wave-induced motions are based on strip-theory, which is accurate when the Froude number given by $\mathrm{Fn} = U/\sqrt{gL}$, is less than 0.3, see (Jensen, 2001). This assumption will generally be the case when the vehicle in consideration is slender and/or the speed U is low, which is the common case for most wave-propelled USVs.

Ignoring the frequency-dependency in the added mass, the seakeeping analysis as stated in (Fossen, 2021) for decoupled motions in heave z^n and pitch θ can be written as a forced mass-damper-spring system on the form

$$M_{33}\ddot{z}^n + B_{33}(\omega,\omega_e)\dot{z}^n + C_{33}z^n = Z_0\,\zeta_a\cos(\omega_e t), \tag{5}$$

$$M_{55}\ddot{\theta} + B_{55}(\omega,\omega_e)\dot{\theta} + C_{55}\theta = M_0\,\zeta_a\sin(\omega_e t), \tag{6}$$

where Z_0 is the forcing function from wave elevation ζ_a to heave and M_0 is the corresponding forcing function in pitch. We observe that the coupled motion in heave and pitch has 90° phase difference (Z_0 and M_0 real). In (Jensen et al., 2004) a constant sectional added mass equal to the displaced water was assumed. From strip-theory, the longitudinal motions for box-shaped vessels are

$$2\frac{k\tilde{T}}{\omega^2}\ddot{\xi} + \frac{R^2}{k\tilde{B}\eta^3\omega}\dot{\xi} + \xi = F_0\,\zeta_a\cos(\omega_e t + \epsilon). \tag{7}$$

Here, ξ is placeholder for heave or pitch, F_0 is the forcing function (Z_0 or M_0), ϵ is the phase angle (0° for heave and 90° for pitch) and R is the dimensionless ratio between incoming and the diffracted wave amplitudes, given by

$$R = 2\sin(0.5k\tilde{B}\eta^2)\exp(-k\tilde{T}\eta^2). \tag{8}$$

Note that the coupled phase of the longitudinal motions is enforced since Eq. (7) has the same left hand side. Hence the relative damping ratio $\zeta_3 = \zeta_5$ and natural frequency $\omega_{n3} = \omega_{n5}$ is equal. This enforces a *loose coupling*.

The dynamical model from Jensen et al. (2004) can be rewritten according to the seakeeping notation in (Fossen, 2021) by restructuring Eq. (7). For a box-shaped vehicle, Fig. 2b, the modelled terms in heave and pitch were found:

- *Heave entries*: Inertia $M_{33} = 2\tilde{\nabla}\rho$, damping $B_{33} = \tilde{L}\frac{\rho g}{k\omega_e}\frac{R^2}{\eta^2}$, and restoring term $C_{33} = \rho g\tilde{L}\tilde{B}$.
- *Pitch entries*: Inertia $M_{55} = 2\rho\tilde{\nabla}\tilde{T}\tilde{\mathrm{GM}}_{\mathrm{L}}$, damping $B_{55} = \tilde{L}\tilde{T}\tilde{\mathrm{GM}}_{\mathrm{L}}\,\frac{\rho g}{k\omega_e}\frac{R^2}{\eta^2}$, and restoring term $C_{55} = \rho g\tilde{\nabla}\tilde{\mathrm{GM}}_{\mathrm{L}}$.

Here, the volume of displaced water is $\tilde{\nabla} = \tilde{L}\tilde{B}\tilde{T}$ and the longitudinal metacentric height is $\tilde{\mathrm{GM}}_{\mathrm{L}} = \frac{1}{12}\tilde{L}^2/\tilde{T}$.

Inspired by Fossen (2021), we re-write the forcing functions Z_0 and M_0 in Jensen et al. (2004) according to

$$Z_0 = C_{33}\,\mathrm{sinc}(\sigma)\kappa f, \tag{9}$$

$$M_0 = C_{55}\frac{6}{\tilde{L}\sigma}\left[\mathrm{sinc}(\sigma) - \cos(\sigma)\right]\kappa f, \tag{10}$$

where $\sigma := \frac{1}{2}k_e\tilde{L}$ and $k_e = k|\cos(\beta)|$ is the effective wave number, $\kappa = \exp(-k_e\tilde{T})$ is the Smith's correction factor, the function $\mathrm{sinc}(x) = \sin(x)/x$ and

$$f = \sqrt{(1 - k\tilde{T})^2 + \left(R^2/(k\tilde{B}\eta^3)\right)^2}.$$

4.3 Roll motion

The roll motion ϕ can be described by

$$M_{44}\ddot{\phi} + B_{44}\dot{\phi} + C_{44}\phi = K_0\,\zeta_{\mathrm{a}}\cos(\omega_e t + \epsilon_\phi), \tag{11}$$

where K_0 is the forcing function from waves and ϵ_ϕ is the phase angle. The moment of inertia is $M_{44} = (T_4/2\pi)^2\,C_{44}$ related to roll time period T_4 and the restoring coefficient $C_{44} = \rho g\tilde{\nabla}\tilde{\mathrm{GM}}_{\mathrm{T}}$. The natural period in roll can as a first guess be approximated by $T_4 \simeq 2\tilde{B}C_{\mathrm{geo}}\tilde{\mathrm{GM}}_{\mathrm{T}}^{-1/2}$ according to the International Maritime Organization (1991) resolution A.685(17). An estimation of the geometric constant C_{geo} based on A.562(14) is $C_{\mathrm{geo}} \simeq 0.373 + 0.023\tilde{B}/\tilde{T}$.

An alternative to the above is to use the method by Jensen et al. (2004) to predict the physics of the roll motion by using a simplified monohull geometry shown in Fig. 2c. This provides alternative geometrical formulations with explicit, however longer expressions. Details of this method is presented in Mounet et al. (2024). A better approximation for the roll dynamics can be found in (Matsui et al., 2023). In (Fossen, 2021) the damping is directly estimated from the relative damping ratio ζ_4 by

$$B_{44} = 2\zeta_4\,(T_4/2\pi)\,C_{44},$$

where the exciting moment due to regular waves is

$$K_0 = \sqrt{(\rho g^2/\omega_e)B_{44}}\,\sin(\beta). \tag{12}$$

4.4 Fluid memory effects in pitch and heave

In the following, closed-form approximation for fluid memory effects in heave and pitch are derived. The entries for roll is zero since this motion was modelled independent of frequency, i.e., matrices $\mathbf{A}_{\mathrm{r}44}$, $\mathbf{B}_{\mathrm{r}44}$ and $\mathbf{C}_{\mathrm{r}44}$ are zero.

By analysing Eq. (8) we introduce the dimensionless frequency $\omega' = \omega(\tilde{B}/2g)^{1/2}$ in order to express the sectional damping $b(\omega') = B_{33}/\tilde{L}$, on ω' and transversal aspect ratio $\Lambda_{\mathrm{T}} := \tilde{B}/\tilde{T}$. From Perez and Fossen (2008), we choose the simplest rational transfer function candidate for the retardation function $K(\mathrm{s})$, or similarly the state-space of the fluid memory effects in Eqs. (3b)–(3c). The function is second order, input-output stable, has zero at $s = 0$ and we base the analysis on $s' = j\omega'$. The fluid memory effects for heave and pitch motions of the box-shaped vessel were first found from Eq. (7) with s' and transferred back;

$$\hat{K}(s) = \frac{\mu_{\mathrm{r}}}{\dot{\xi}}(s) = \frac{2\rho\tilde{B}g\sqrt{2g/\tilde{B}}\cdot q_0'\cdot C_{\mathrm{motion}}\,s}{s^2 + \sqrt{2g/\tilde{B}}\cdot p_1'\,s + (2g/\tilde{B})\cdot p_0'}, \tag{13}$$

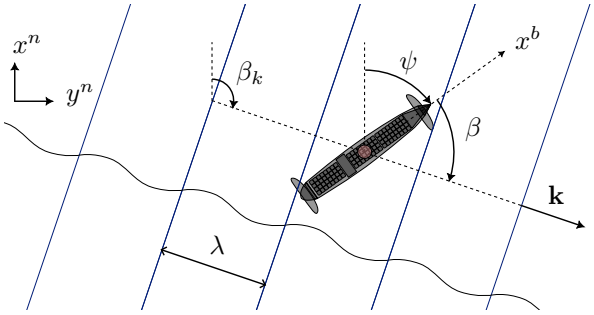

Fig. 3. Definition of wave encounter angle, $\beta = \beta_k - \psi$.

where the motion constant is different for pitch and heave,

$$C_{\text{motion}} = \{\tilde{L};\ \text{for heave}, \quad \tilde{L}\tilde{T}\tilde{\text{GM}}_{\text{L}};\ \text{for pitch}\}.$$

The parameters q_0', p_0' and p_1' in Eq. (13) depend on the geometry, and were found by a least-square fit from K found from Ogilvie's transformation of Eq. (7) where we used $b(\omega) = \rho g^2 R(\omega)^2/\omega^3$. They are reported as ($\Lambda_{\text{T}}$>1):

$$q_0'(\Lambda_{\text{T}}) \simeq 0.5696 \cdot \frac{\Lambda_{\text{T}} - 0.018}{\Lambda_{\text{T}} + 1.035}, \tag{14a}$$

$$p_0'(\Lambda_{\text{T}}) \simeq 0.5917 \cdot \frac{\Lambda_{\text{T}} - 0.245}{\Lambda_{\text{T}} + 0.612}, \tag{14b}$$

$$p_1'(\Lambda_{\text{T}}) \simeq 0.7376 \cdot \frac{\Lambda_{\text{T}} + 0.394}{\Lambda_{\text{T}} + 0.642}. \tag{14c}$$

A realization of the fluid memory effects in Eq. (13) is

$$\mathbf{A}_{\text{r},33} = \mathbf{A}_{\text{r},55} = \begin{bmatrix} -\sqrt{2g/B}\, p_1'(\Lambda_{\text{T}}) & -(2g/B)\, p_0'(\Lambda_{\text{T}}) \\ 1 & 0 \end{bmatrix},$$

$$\mathbf{B}_{\text{r},33} = \mathbf{B}_{\text{r},55} = \begin{bmatrix} 1,\ 0 \end{bmatrix}^\top,$$

$$\text{and} \quad \mathbf{C}_{\text{r},33} = \mathbf{C}_{\text{r},55} = \begin{bmatrix} 2\rho g \sqrt{2Bg}\, C_{\text{motion}}\, q_0'(\Lambda_{\text{T}}),\ 0 \end{bmatrix}.$$

• *First order wave force transfer functions*: Denoting $\boldsymbol{\tau}_0(\omega_e) = [Z_0(\omega_e), K_0(\omega_e)s, M_0(\omega_e)]^\top$ as the frequency-dependent forcing function (+90° phase in K_0), first order wave forces from wave amplitude $\zeta_{\text{a},i}$ and phase ϵ_i are:

$$\boldsymbol{\tau}_{\text{wave1}} := \sum_{i=1}^{\infty} \boldsymbol{\tau}_0(\omega_{e,i}) \zeta_{\text{a},i} \cos(\omega_{e,i} t + \epsilon_i) \tag{15}$$

5. FOIL PROPULSION MODEL

The following sections show that foil dynamics are described by a mass-damper-spring model in subsystem Σ_3;

$$\mathbf{M}_\vartheta \ddot{\boldsymbol{\vartheta}}_{\text{n}} + \mathbf{B}_\vartheta(\dot{\boldsymbol{\vartheta}}_{\text{n}})\dot{\boldsymbol{\vartheta}}_{\text{n}} + \mathbf{C}_\vartheta(\boldsymbol{\vartheta})\boldsymbol{\vartheta}_{\text{n}} = \cdots \tag{16a}$$

$$\mathbf{C}_\vartheta(\boldsymbol{\vartheta})\mathbb{I}_{N\times 1}\theta + \mathbf{Q}_{\text{A}} + \mathbf{Q}_{\text{N}} + \mathbf{Q}_{\text{inertia}}(\ddot{\mathbf{x}}_{\text{p}}^n, \ddot{\mathbf{z}}_{\text{p}}^n),$$

$$\dot{\mathbf{x}}_{\text{t}} = \mathbf{A}_{\text{t}}(\mathbf{U}_{\text{r}})\mathbf{x}_{\text{t}} + \mathbf{B}_{\text{t}}\mathbf{Q}_{\text{N,stationary}}, \tag{16b}$$

$$\mathbf{Q}_{\text{N}} = \mathbf{C}_{\text{t}}(\mathbf{U}_{\text{r}})\mathbf{x}_{\text{t}} + \mathbf{D}_{\text{t}}\mathbf{Q}_{\text{N,stationary}}, \tag{16c}$$

where the vector $\boldsymbol{\vartheta}_n = [\vartheta_{n,1}, ..., \vartheta_{n,m}]^\top$ contains all m foil angles relative to NED such that ϑ_i is the foil angle relative to the body frame and $\vartheta_{n,i} = \theta + \vartheta_i$. The foil angle ϑ is measured relative to the USV body with positive direction following y^b-axis. The matrices $\mathbf{M}_\vartheta$, $\mathbf{B}_\vartheta$ and $\mathbf{C}_\vartheta$ represents mass-damper-spring terms for the foils (on the diagonal entries) modelled as low-frequency motion, see Sect. 5.8. The moment vectors contain the respective added mass moments $\mathbf{Q}_{\text{A}} = [Q_{A,1}, ..., Q_{A,m}]^\top$ and likewise for transient lift and drag moments $\mathbf{Q}_{\text{N}}$ filtered by "*fluid-memory-like*" matrices $\mathbf{A}_{\text{t}}$–$\mathbf{D}_{\text{t}}$ of the correct stationary moment $\mathbf{Q}_{\text{N,stationary}}$. We denote relative velocities of the pivot points by $\mathbf{U}_{\text{r}} = [U_{\text{r},1}, ..., U_{\text{r},m}]^\top$. For inertial correction $\mathbf{Q}_{\text{inertia}}$, their accelerations $\ddot{\mathbf{x}}_{\text{p}}^n$ and $\ddot{\mathbf{z}}_{\text{p}}^n$ is needed.

The parameters in subsystem Σ_3 may include the foil span S, the mean chord length c_m, foil force characteristics described by α_s, C_{Ls}, C_{Ds} and Δ_s (defined later) and positions of the pivot point x_{p} and centre of mass $x_{\text{c.g.}}$ along the chord length (parameters for each foil needed):

$$\boldsymbol{\alpha}_3 = \big(S, c_m, \alpha_s, C_{Ls}, C_{Ds}, \Delta_s, x_{\text{p}}, x_{\text{c.g.}}, \text{etc.}\big)$$

5.1 Uncorrected analytical quasi-steady lift and drag forces

A foil in stationary flow U_{r} will experience lift L, drag D force according to Fig. 4. The suction force and viscous drag is neglected in this study, thus we can write the normal force magnitude as $N = \sqrt{L^2 + D^2}$. From linear foil theory, the analytical quasi-steady forces on the foils, whose magnitude is valid for small angles and qualitatively correct for larger angles, are (per length; see Tufte (2024))

$$L'(\alpha) = (1/2)\rho U_r^2 c\, \pi \sin(2\alpha), \tag{17a}$$

$$D'(\alpha) = (1/2)\rho U_r^2 c\, 2\pi \sin(\alpha)^2. \tag{17b}$$

Here, the relative water velocity is U_r, foil chord length c and attack angle is α, where $\alpha = 0°$ is head on. For relative velocities $\mathbf{U}_{\text{r}}^b = [u_{\text{r}}, v_{\text{r}}, w_{\text{r}}]^\top$, then $\alpha = \arctan(w_{\text{r}}, u_{\text{r}}) + \vartheta$.

5.2 Centre of pressure at non-modelled operating points

For small attack angles, the centre of pressure appears at the quarter-chord position from leading edge, which can be found analytically. It is more or less valid up to the stall angle. However, at larger angles the flow detaches and the centre of pressure depends on the attack angle. We use a piecewise continuous approximation

$$x_{\text{c.p.}}(\alpha) = \begin{cases} 1/4, & |\alpha| \le 0.05\pi, \\ 1/5 + 1/\pi \cdot |\alpha|, & 0.05\pi < |\alpha| \le 0.20\pi, \\ 1/3 + 1/3\pi \cdot |\alpha|, & 0.20\pi < |\alpha| \le 0.80\pi, \\ -1/5 + 1/\pi \cdot |\alpha|, & 0.80\pi < |\alpha| \le 0.95\pi, \\ 3/4, & 0.95\pi < |\alpha| \end{cases} \tag{18}$$

from experimental and numerical investigation for flat plates in uniform inflow stream by Mirzaeisefat (2011).

5.3 Correcting for three-dimensional effects

To correct for three-dimensional effects, a correction coefficient $C_{3D}(\Lambda)$ is added based on aspect ratio $\Lambda = S/c_m$. A blend from literature, e.g., Prandtl's lifting line theory, aerospace or rudders, correct for $\Lambda \to \infty$ is proposed:

$$C_{3D}(\Lambda) = \frac{\Lambda}{\Lambda + 2.25}. \tag{19}$$

5.4 Correcting for stall

The effect of stall introduces a sudden reduction in lift and increase in drag beyond the stall angle α_s. This is due to unattached flow, and is of importance for modelling foils in wave-propelled vehicles due to low speeds and large attack angles. By multiplying the lift and drag forces by non-dimensional coefficients $C_{Ln}(\alpha)$ and $C_{Dn}(\alpha)$, this effect is incorporated. We propose a simplified model for the stall effect with a sigmoid blending function $\sigma_s(\alpha, \alpha_s) \in [0, 1]$, mid-point given by the second argument. The model is

$$C_{Ln}(\alpha) = 1 - C_{Ls}\sigma_s(|\alpha|, \alpha_s) + C_{Ls}\sigma_s(|\alpha|, \pi - \alpha_s), \tag{20}$$

$$C_{Dn}(\alpha) = C_{Ds}\big[1 + C_{Ls}\sigma_s(|\alpha|, \alpha_s) - C_{Ls}\sigma_s(|\alpha|, \pi - \alpha_s)\big]. \tag{21}$$

For practical considerations, fluttering phenomena can be reduced in the model by widening the blending function σ_s, which correspond to increasing Δ_s if one uses

$$\sigma_s(x, x_0; \Delta_s) = 1/(1 + \exp(-10(x - x_0)/\Delta_s)),$$

where Δ_s is the interval for 0.01–0.99 rise.

5.5 Transient lift and drag forces

The work of Theodorsen (1949) showed analytically that lift and drag forces on thin foils are frequency-dependent based on the reduced frequency $k_f := 0.5\, c_m \cdot (\omega_f/U_{\text{r}})$ where ω_f is the frequency of oscillation of the foil.

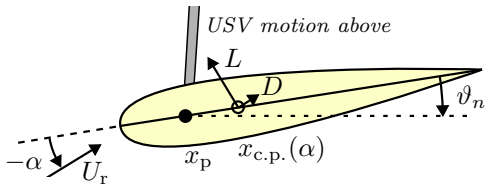

Fig. 4. Lift L and drag D forces on a foil in steady relative flow U_r at an attack angle α. Modelled by angle ϑ_n.

Theodorsen introduced the complex factor $C_{\text{Th}}(k_f)$ for adding a phase and attenuation to the lift and drag forces. The coefficient however involves complex calculations with Hankel functions and is therefore unsuited for simulation purposes. A second-order transfer function with reasonable agreement for the entire frequency range is proposed:

$$\hat{C}_{\text{Th}}(s') = \frac{0.5\,s'^2 + 0.549\,s' + 0.095}{s'^2 + 0.848\,s' + 0.095} \tag{22}$$

with $s' = jk_f$. Notice that the Laplace variable is based on the reduced frequency, $s' = jk_f$. When applying the above, one needs to substitute the variable $s = (2U_r/c_m)s'$ to obtain a velocity-dependent model of non-stationary forces. This results in the linear-time-variant state-space approximation based on the inflow velocity.

The corrected, non-stationary lift and drag forces are

$$L = \hat{C}_{\text{Th}}(s)L'(\alpha)C_{3D}(\Lambda)C_{Ln}(\alpha)\cdot S, \tag{23a}$$

$$D = \hat{C}_{\text{Th}}(s)D'(\alpha)C_{3D}(\Lambda)C_{Ln}(\alpha)\cdot S. \tag{23b}$$

The sub-matrices for the state-space approximation of the transient in Eqs. (16b)–(16c) for foil i is ($s = (2U_r/c_m)s'$):

$$\mathbf{A}_{t,ii} = \begin{bmatrix} -1.696\,U_{r,i}/c_{m,i} & -0.380\,(U_{r,i}/c_{m,i})^2 \\ 1 & 0 \end{bmatrix}, \quad \mathbf{B}_{t,ii} = \begin{bmatrix} 1 \\ 0 \end{bmatrix},$$

$$\mathbf{C}_{t,ii} = \begin{bmatrix} 0.250\,U_{r,i}/c_{m,i}, & 0.190\,(U_{r,i}/c_{m,i})^2 \end{bmatrix}, \text{ and } D_{t,ii} = 0.5.$$

5.6 Added mass forces and moments

The added mass force (per unit span) is modelled by the normal component of the expression for infinite thin plates

$$A' = (1/4)\rho\pi c^2 \dot{U}_r \sin(\alpha_{\text{acc}}), \tag{24}$$

where $\dot{U}_r$ is the relative inflow acceleration, attack angle $\alpha_{\text{acc}} = \arctan(\dot{w}_r, \dot{u}_r) + \vartheta$ and assumed to act through the centre (Meyerhoff, 1970). To correct for three-dimensional effects, we suggest to use the following formula ($\Lambda > 1$)

$$C_a(\Lambda) = \frac{\Lambda - 0.260}{\Lambda + 0.290}, \tag{25}$$

to match the analytical results by Meyerhoff (1970). The corrected added-mass force is thus $A = A'C_a(\Lambda)\cdot S$. The added moment of inertia along the half-chord point is

$$Q'_{\ddot{\vartheta}} = J'_a = (1/128)\rho\pi c_m^4, \tag{26}$$

according to Lamb (1916), which should be slightly higher for rotation about the pivot point, $Q_{\ddot{\vartheta}} = J_a \geq Q'_{\ddot{\vartheta}}\cdot S$.

5.7 Passive spring moments for optimal wave-propulsion

The restoring moment of the foils by passive springs ensures that the USV and foils interact in an optimal manner for wave propulsion. The spring moment is modelled with $-Q_\vartheta(\vartheta)\vartheta$, e.g., linear if torsion springs are employed.

5.8 Individual foil dynamical model and propulsion forces

Assuming that the foils are driven by pitch and heave motion of the USV, with no roll coupling for slowly heading rate, we found the rotational dynamics around the pivot point x_p (distances from nominal leading edge, see Fig. 4):

$$\begin{aligned}
J_p\ddot{\vartheta}_n = &- Q_{\ddot{\vartheta}}\ddot{\vartheta}_r && \text{(rotational inertia)}\\
&- Q_{\dot{\vartheta}}(\dot{\vartheta}_r)\dot{\vartheta}_r && \text{(rotational damping)}\\
&- Q_\vartheta(\vartheta)\vartheta && \text{(spring moment)}\\
&+ N\cdot(x_{c.p.}(\alpha) - x_p) && \text{(lift and drag forces)}\\
&+ A\cdot(0.5c_m - x_p) && \text{(added mass force)}\\
&+ D_v\sin(\alpha)\cdot(0.5c_m - x_p) && \text{(viscous damping)}\\
&+ B\cos(\vartheta_n)\cdot(x_{c.b.} - x_p) && \text{(buoyancy)}\\
&- G\cos(\vartheta_n)\cdot(x_{c.g.} - x_p), && \text{(gravity)}\\
&- \ddot{Z}_p\cos(\vartheta_n)\cdot(x_{c.g.} - x_p) && \text{(inertia correction)}\\
&- \ddot{X}_p\sin(\vartheta_n)\cdot(x_{c.g.} - x_p) && \text{(inertia correction)}
\end{aligned}$$

Here, ϑ is the foil angle relative to the vehicle, hence $\vartheta_n = \theta + \vartheta$ is relative to NED, and $\dot{\vartheta}_r$ is the relative rotation velocity which was set equal to $\dot{\vartheta}_n$. The moment of inertia of the foil around the pivot point is J_p, centre of buoyancy is $x_{c.b.}$ and centre of gravity is $x_{c.g.}$. We denote $\ddot{Z}_p$ and $\ddot{X}_p$ as the combined acceleration times foil mass in z^n- and x^n-direction of the pivot point, which can be found through kinematics of the USV seakeeping motion.

• *Single uncoupled foil dynamics*: Assuming that the contribution from gravity and buoyancy cancels, and incorporating viscous damping into damping moment for tuning considerations (damping relies on the specific foil), the dynamics is re-written as a mass-damper-spring system:

$$M_\vartheta\ddot{\vartheta}_n + B_\vartheta\dot{\vartheta}_n + C_\vartheta\vartheta_n = C_\vartheta\theta + Q_N + Q_A + Q_{\text{inertia}} \tag{27}$$

Here, $M_\vartheta = J_p + Q_{\ddot{\vartheta}}$, $B_\vartheta = Q_{\dot{\vartheta}}(\dot{\vartheta}_n)$, $C_\vartheta = Q_\vartheta(\vartheta)$, the transient lift and drag forces $Q_N = N\cdot(x_{c.p.}(\alpha) - x_p)$ by filtering $Q_{N,\text{stationary}}$, added mass $Q_A = A\cdot(0.5c_m - x_p)$ and inertia moment Q_{inertia} as defined above.

• *Wave-propulsion*: Finally, the propulsive forces are

$$\boldsymbol{\tau}_{\text{foil}} = \begin{bmatrix} X_{\text{foil}} \\ Y_{\text{foil}} \\ N_{\text{foil}} \end{bmatrix} := \sum_{i=1}^{m} \begin{bmatrix} (N_i + A_i)(1 - t_{F,i})\sin(\vartheta_{n,i}) \\ 0 \\ 0 \end{bmatrix}, \tag{28}$$

which follows from the induced lift, drag and added mass forces on the foil surface, ignoring roll; else $Y_{\text{foil}}, N_{\text{foil}} \neq 0$. We add $t_F \simeq 0.05$–0.5 as a resistance coefficient similar to the convention used in rudder theory, to be tuned.

6. CASE STUDY: AUTONAUT

We employ the proposed system architecture on a 5.0 m length version of the AutoNaut vehicle from Norwegian University of Science and Technology (NTNU). The vehicle consists of one simple foil at the fore and a port-starboard decoupled foil at the aft. The main particulars for the vehicle is listed in Tab. 1 (Tufte, 2024). The manoeuvring terms, wind and steering parameters of this particular vehicle was found by Dallolio et al. (2022b).

Table 1. Main particulars NTNU AutoNaut.

Main particulars		**Unit**
Length, L (L_{pp})	5.0 (4.6)	[m]
Breadth, B	0.8	[m]
Draft, T (w/foils)	0.3 (0.8)	[m]
Foil span, S	1.3	[m]
Mean chord length, c_m	0.192	[m]

• *Seakeeping model*: Mounet et al. (2024) has validated subsystem Σ_2 by optimizing the response spectra for a range of experimental sea trials. The parameters for $\boldsymbol{\alpha}_2$ is reported as $\tilde{L} = 6.146$ m, $\tilde{B} = 1.236$ m and $\tilde{T} = 0.287$ m.

• *Propulsion model*: The physical parameters for the foil placement, dimensions and force characteristics has been measured and listed in detail by Tufte (2024). The lift and drag curve parameters $\alpha_s, C_{Ls}, C_{Ds}, \Delta_s$, Eqs. (23a)–(23b), was optimized with panel method software.

6.1 Simulations and course control demonstration

• *Simulation*: The effect of spring stiffness (Tufte, 2024) is shown in Fig. 5, and suggest that soft springs are suited for wave-propulsion at wave frequencies $\omega < 1.4$ rad/s, the medium setting at $\omega = 1.4$–2.2 rad/s and the stiff springs are most efficient for short-crested sea, at $\omega > 2.2$ rad/s.

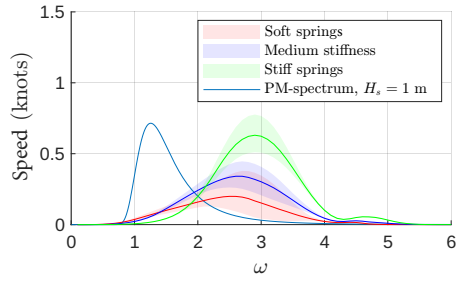

Fig. 5. Forward speed prediction with different spring settings. The results should be analysed with respect to the wave frequencies present, e.g., the Pierson-Moskowitz spectrum, (units not shown).

• *Control example*: Additionally, a line of sight (LOS) course control was simulated in Fig. 6. The controller gains $K_p = 1.0$, $K_i = 0.05$ and $K_d = 10$ gave satisfactory results.

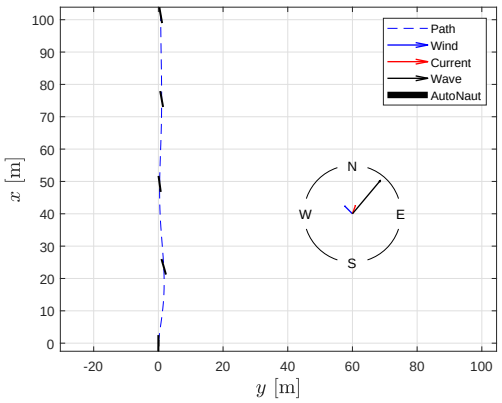

Fig. 6. LOS course control simulation for 200 seconds. Wave height 0.5 m, wave frequency $\omega = 2.5$ rad/s, propagation direction $\beta_k = 40°$. Current (0.2 m/s) and wind (2.5 m/s) directions shown in compass rose.

• *On validation*: While the framework successfully integrates closed-form models, further validation is needed across a range of operational scenarios. Future work should in detail describe the final model validated to experimental data, and compare to data-driven prediction in Øveraas et al. (2022) or similar studies. Exploring nonlinear damping, and a fully coupled model would improve predictive accuracy for advanced guidance and control development.

7. CONCLUSION

This paper has presented a unified modelling framework for predicting the motion of wave-propelled uncrewed surface vehicles (USVs) using closed-form expressions. By decomposing the system into manoeuvring dynamics, wave induced responses, and foil dynamics, the model captures essential physical interactions and wave-propulsion in a computationally efficient manner. The feasibility of the approach was demonstrated through application to a 5.0 m AutoNaut platform with partly validated parameters and a simulated course control example. The results support the model's potential use for early-stage control design and decision-support systems for wave-propelled USVs.

Future work should consider experimental validation under varying sea states and possible test various use cases. Accounting for nonlinear damping, unsteady hydrodynamic effects and coupling in more detail could improve accuracy in high sea states or aggressive manoeuvres.

ACKNOWLEDGEMENTS

We thank Alberto Dallolio and Henning Øveraas for providing data and information on the AutoNaut platform. The work was in part supported by the Research Council of Norway, project Autoteaming (344326).

REFERENCES

Brix, J. (1993). *Manoeuvring Technical Manual*. Seehafen Verlag, Hamburg.

Bøckmann, E. (2015). *Wave Propulsion of Ships*. Ph.D. thesis, Norwegian University of Science and Technology.

Dallolio, A., Øveraas, H., and Johansen, T.A. (2022a). Gain-scheduled steering control for a wave-propelled unmanned surface vehicle. *Ocean Eng.*, 257, 111618.

Dallolio, A. et al. (2022b). Design and validation of a course control system for a wave-propelled unmanned surface vehicle. *Field Robotics*, 2(1), 748–773.

Fossen, T.I. (2005). A nonlinear unified state-space model for ship maneuvering and control in a seaway. *Int. Journal of Bifurcation and Chaos*, 15(9), 2717–2746.

Fossen, T.I. (2021). *Handbook of marine craft hydrodynamics and motion control*. Wiley, 2nd edition.

International Maritime Organization (1991). Resolutions A.749(18) and A.562(14).

Jensen, J.J. (2001). *Load and Global Response of Ships*, chapter 4: Wave Loads on Ships. Elsevier, 4th edition.

Jensen, J.J., Mansour, A.E., and Olsen, A.S. (2004). Estimation of ship motions using closed-form expressions. *Ocean Engineering*, 31(1), 61–85.

Kijima, K., Katsuno, T., Nakiri, Y., and Furukawa, Y. (1990). On the manoeuvring performance of a ship with the parameter of loading condition. *Journal of The Society of Naval Architects of Japan*, 168, 141–148.

Kristiansen, E. and Egeland, O. (2003). Frequency-dependent added mass in models for controller design for wave motion damping. *IFAC Proc.*, 36(21), 67–72.

Lamb, H. (1916). *Hydrodynamics*. Cambridge University Press, Cambridge, 4th edition.

Matsui, S. et al. (2023). Simplified estimation formula for frequency response function of roll motion of ship in waves. *Ocean Engineering*, 276, 115212.

Meyerhoff, W.K. (1970). Added masses of thin rectangular plates calculated from potential theory. *Journal of Ship Research*, 14(2), 100–111.

Mirzaeisefat, S. (2011). *Fluttering and Autorotation of Hinged Vertical Flat Plate Induced by Uniform Current*. Ph.D. thesis, University of Michigan.

Mounet, R.E.G. et al. (2024). Data-driven method for hydrodynamic model estimation applied to an unmanned surface vehicle. *Measurement*, 234, 114724.

Ogilvie, T.F. (1964). Recent progress toward the understanding and prediction of ship motions. *Proceedings of the 5th Symposium on Naval Hydrodynamics*, 3–80.

Perez, T. and Fossen, T.I. (2008). Joint identification of infinite-frequency added mass and fluid-memory models of marine structures. *MIC Journal*, 29(3), 93–102.

Theodorsen, T. (1949). General theory of aerodynamic instability and the mechanism of flutter. NACA-TR-496, National Aeronautics and Space Administration.

Tufte, A.G. (2024). Predicting motion of wave-propelled USVs using closed form expressions. Master's thesis, Norwegian University of Science and Technology.

Øveraas, H., Heggernes, A., Dallolio, A., Bryne, T.H., and Johansen, T.A. (2022). Predicting the speed of a wave-propelled autonomous surface vehicle using metocean forecasts. *IEEE/MTS OCEANS Conference, Chennai.*